PHYSICAL REVIEW B **92**, 100404(R) (2015)

High antiferromagnetic transition temperature of the honeycomb compound $SrRu_2O_6$

W. Tian,[1] C. Svoboda,[2] M. Ochi,[3] M. Matsuda,[1] H. B. Cao,[1] J.-G. Cheng,[4] B. C. Sales,[5] D. G. Mandrus,[5,6] R. Arita,[3] N. Trivedi,[2] and J.-Q. Yan[5,6]

[1]*Quantum Condensed Matter Division, Oak Ridge National Laboratory, Oak Ridge, Tennessee 37831, USA*

[2]*Department of Physics, Ohio State University, Columbus, Ohio 43210, USA*

[3]*RIKEN Center for Emergent Matter Science, 2-1 Hirosawa, Wako, Saitama 351-0198, Japan*

[4]*Beijing National Laboratory for Condensed Matter Physics, and Institute of Physics, Chinese Academy of Sciences, Beijing 100190, People's Republic of China*

[5]*Materials Science and Technology Division, Oak Ridge National Laboratory, Oak Ridge, Tennessee 37831, USA*

[6]*Department of Materials Science and Engineering, University of Tennessee, Knoxville, Tennessee 37996, USA*

(Received 14 April 2015; published 14 September 2015)

We study the high-temperature magnetic order in a quasi-two-dimensional honeycomb compound $SrRu_2O_6$ by measuring magnetization and neutron powder diffraction with both polarized and unpolarized neutrons. $SrRu_2O_6$ crystallizes into the hexagonal lead antimonate ($PbSb_2O_6$, space group $P\bar{3}1m$) structure with layers of edge-sharing RuO_6 octahedra separated by Sr^{2+} ions. $SrRu_2O_6$ is found to order at $T_N = 565$ K with Ru moments coupled antiferromagnetically both in plane and out of plane. The magnetic moment is 1.30(2) μ_B/Ru at room temperature and is along the crystallographic c axis in the G-type magnetic structure. We perform density functional calculations with constrained random-phase approximation (RPA) to obtain the electronic structure and effective intra- and interorbital interaction parameters. The projected density of states shows strong hybridization between Ru $4d$ and O $2p$. By downfolding to the target t_{2g} bands we extract the effective magnetic Hamiltonian and perform Monte Carlo simulations to determine the transition temperature as a function of inter- and intraplane couplings. We find a weak interplane coupling, 3% of the strong intraplane coupling, permits three-dimensional magnetic order at the observed T_N.

DOI: 10.1103/PhysRevB.92.100404 PACS number(s): 75.30.Et, 71.15.Mb, 75.47.Lx, 75.50.Ee

It is evident that for the design of the next generation of multifunctional devices, we need new paradigms, new principles, and new classes of materials. Magnetism is arguably the most technologically important property arising from electron interactions. One of the central questions has been how to create magnetic materials with high transition temperatures T_c for room-temperature devices. Broadly two paradigms define the formation of the magnetic state starting with fermions at finite temperatures: For weak Coulomb interactions U/W compared to the bandwidth, one expects a Fermi liquid at finite temperatures, followed by a Fermi surface nesting instability that opens a gap in the spectrum, resulting in a Slater antiferromagnet below $T_c \sim We^{-c\sqrt{W/U}}$, which is exponentially suppressed in the coupling (c is a constant). In the opposite regime for $U/W \gg 1$, local moments form on a much higher temperature scale $T^* \approx U$ opening a large Mott gap and order on the scale of antiferromagnetic (AF) superexchange $J \sim W^2/U$. The transition temperature as a function of U/W reaches its maximum in the fluctuating regime with $U \approx W$. $SrTcO_3$ is currently believed to be at the maximum with a $T_c \approx 1000$ K [1–6]. Tuning U/W by combining different $3d$ and $5d$ ions in double perovskites also increases T_c well above room temperature [7], as in Sr_2CrReO_6 with $T_c = 635$ K [8] and in Sr_2CrOsO_6 with $T_c = 720$ K [9]. These are examples of Mott-Hubbard antiferromagnetic insulators. $NaOsO_3$ orders at $T_c = 410$ K [10,11], which is a rare example of Slater insulator approaching the fluctuating region from the itinerant side. All the above reported high-T_c compounds have perovskite structures with a d^3 electronic configuration. Experimental studies of these interesting osmates and technetium compounds have been impeded by the safety concerns from toxic osmium oxide (mainly OsO_4) and radioactive technetium.

Recently, a metastable compound $SrRu_2O_6$ with a quasi-two-dimensional structure was proposed to order antiferromagnetically with T_N above 500 K [12]. $SrRu_2O_6$ crystallizes into the hexagonal lead antimonate ($PbSb_2O_6$) structure with the space group $P\bar{3}1m$. As shown in the inset of Fig. 1, the structure consists of layers of edge-sharing RuO_6 octahedra separated by Sr^{2+} ions sitting in the oxygen octahedral interstices. In the *ab* plane, the Ru ions form a honeycomb array. In the previous study [12], the magnetization was measured up to 500 K without finding a signature for the magnetic transition, though the room temperature neutron powder diffraction observed extra reflections absent in x-ray measurements.

In this Rapid Communication, we report our magnetic and neutron diffraction study of $SrRu_2O_6$ up to 750 K. Our diffraction measurements with both polarized and unpolarized neutrons confirm that $SrRu_2O_6$ orders antiferromagnetically at $T_N = 565$ K with a room temperature magnetic moment of 1.30(2) μ_B/Ru along the c axis. The magnetic measurements suggest that strong two-dimensional magnetic correlations persist above T_N as highlighted by the T-linear behavior in Fig. 1 above the kink. We discuss below band structure calculations that show strong Ru $4d$ and O $2p$ hybridization, the role of different exchange pathways, and the derivation of an effective model with in-plane and interplane magnetic interactions to explain the mechanisms and high ordering temperature of $SrRu_2O_6$.

We synthesize polycrystalline $SrRu_2O_6$ by a hydrothermal technique as reported previously [12]. Figure 1 shows the temperature dependence of magnetic susceptibility measured

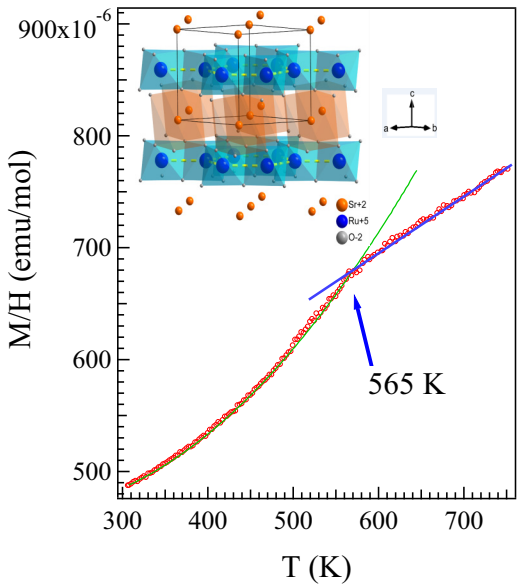

FIG. 1. (Color online) Magnetic susceptibility in the temperature range 300 K $\leqslant T \leqslant$ 750 K measured upon cooling in an applied field of 50 kOe. The solid curves highlight the slope change at 565 K. Inset shows the crystal structure.

in the temperature range 300 K $\leqslant T \leqslant$ 750 K using a quantum design magnetic property measurement system. The data collected in warming and cooling processes overlap, suggesting little or no sample decomposition below 750 K. Above room temperature, the magnetic susceptibility increases with increasing temperature. As highlighted by the solid curves, there is a slope change at 565 K, which signals possible long-range magnetic order.

To study the nature of this slope change, we carry out neutron diffraction experiments in the temperature range 40 K $\leqslant T \leqslant$ 600 K [13]. As shown in Fig. 2(a), neutron powder diffraction observed reflections that are absent in the x-ray powder diffraction pattern. To confirm the magnetic origin of these extra reflections, we perform diffraction measurements using polarized neutrons. With the spin flipper off or on, we measured both the (++) non-spin-flip and the (−+) spin-flip scattering of (1 0 0.5) and (1 0 1), respectively [Figs. 2(b) and 2(c)]. As discussed in Refs. [13–16], the strong scattering detected in the (−+) spin-flip channel confirmed the magnetic origin of the (1 0 0.5) peak.

The diffraction study with polarized neutrons clearly shows that the extra reflections come from a long-range magnetic order instead of any structural transition. Those extra reflections can be indexed on the basis of the magnetic scattering with a G-type AF structure with the magnetic moment direction along the crystallographic *c*-axis. The Rietveld refinement of the neutron diffraction patterns [13] yields a magnetic moment of 1.30(2) μ_B/Ru at 300 K. The magnetic moment increases slightly to 1.34(3) μ_B/Ru upon cooling to 40 K. The moment is smaller than the spin moment of 3 μ_B expected for a half-filled t_{2g} band, which signals a strong covalency of the Ru-O bonds.

As shown in Fig. 2(d), the (1 0 0.5) magnetic peak disappears around 565 K, where a slope change is observed in Fig. 1

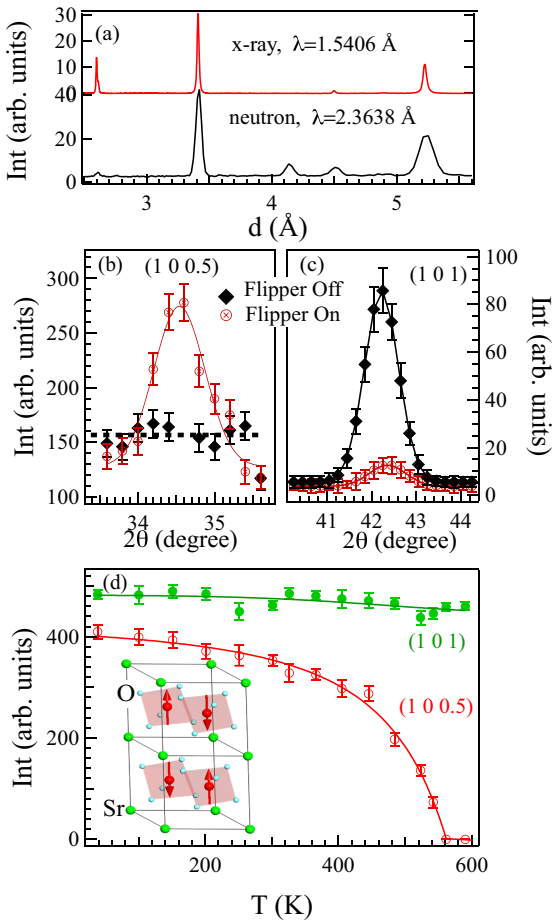

FIG. 2. (Color online) (a) Room-temperature x-ray and neutron powder diffraction patterns in a narrow *d* range, highlighting the extra reflections observed by neutron diffraction. Panels (b) and (c) show the (1 0 0.5) magnetic and (1 0 1) nuclear peaks measured with the polarized neutron in the horizontal field configuration $P_0 \parallel Q$ at room temperature, respectively. The observed weak intensity in panel (c) with the flipper on comes from the finite instrumental flipping ratio, which we estimate to be 1/10 by comparing the integrated intensity of the (−+) and (++) scans of (1 0 1). (d) The temperature dependence of integrated intensity of (1 0 0.5) and (1 0 1) peaks. The solid curves are a guide to the eye. Inset shows the G-type magnetic structure.

in the temperature dependence of the magnetic susceptibility. Figure 2(d) also shows the evolution with temperature of the integrated intensity of the (1 0 1) nuclear peak, which shows little temperature dependence. The coincidence of the disappearance of (1 0 0.5) magnetic peak and the slope change in magnetic susceptibility suggests that a G-type long-range magnetic order takes place at 565 K in $SrRu_2O_6$.

In $SrRu_2O_6$ the Ru ions are in a d^3 electronic configuration in edge-sharing octahedral cages formed by the O atoms. In the presence of correlations, we expect this half-filled system in the t_{2g} manifold to be a Mott insulator. It is important to note that the Ru-O-Ru bond angle is close to 90° and hence both ferromagnetic (F) and AF mechanisms through intermediate oxygens are active in fourth-order processes according to Goodenough-Kanamori rules [17,18]. There are three competing processes that contribute to the exchange

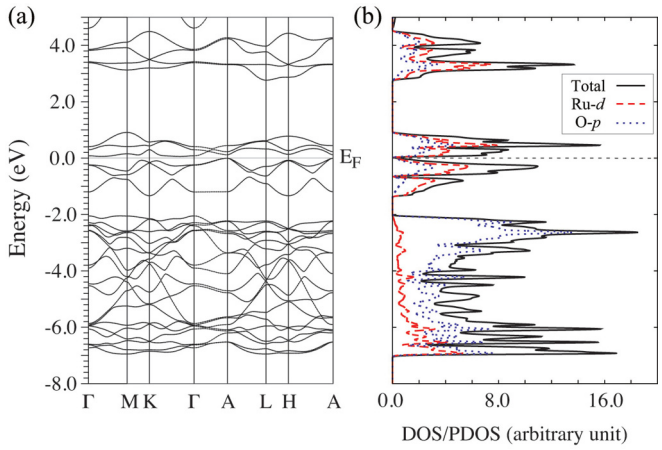

FIG. 3. (Color online) (a) Band dispersion and (b) (projected) density of states for the nonmagnetic state.

interaction: (a) the direct overlap of the half-filled t_{2g} orbitals produces a second-order AF interaction. (b) The transfer of electrons between an oxygen p_z orbital and Ru d_{zx} and d_{yz} orbitals on two neighboring Ru atoms results in an AF superexchange coupling. (c) The transfer of electrons between Ru t_{2g} orbitals and mutually orthogonal oxygen p orbitals results in a F interaction driven by Hund's coupling on oxygen.

It is rather intriguing that $SrRu_2O_6$ orders at such a high temperature, given the competing magnetic interactions. To estimate the relative magnitude of the above competing interactions and to understand the mechanism for the high AF ordering temperature, we perform DFT calculations including constrained RPA to obtain effective hopping and interaction parameters. We also perform spin density functional calculation with the WIEN2K [19] package using the exchange-correlation functional proposed by Perdew *et al.* [20] and the full-potential linearized augmented plane-wave method including the spin-orbit coupling. In the calculation, we use the experimental lattice parameters and atomic configurations determined at room temperature [12].

Our DFT calculation shows that the G-type AF state is the most stable. The nonmagnetic (NM) and the C-type AF (i.e., AF in the ab plane and F along the c axis) states have higher energy than that for the G-type AF state, and there is no ferromagnetic or A-type AF (i.e., F in the ab plane and AF along the c axis) metastable solution. These results indicate that there is a strong in-plane AF correlation compared with that for the out-of-plane direction. Calculated local spin magnetic moment of Ru atoms is about 0.9 μ_B per atom for the G-type AF state and in reasonable agreement with our experiment. Figure 3 shows the band dispersion and (projected) density of states (DOS) for the NM state. The t_{2g} bands [21] are well isolated from the e_g and oxygen p bands. Strong Ru-O hybridization is seen in the DOS, which points to the origin of the reduced local spin magnetic moment of Ru atoms. Possible quantum fluctuations arising from the quasi-two-dimensional structure and orbital fluctuations may also suppress the magnetic moment, but their contribution should be small. The band dispersions of the NM and AF phases are very similar; the NM state has a small band gap of 0.05 eV, which increases to 0.14 eV in the G-type AF state [13].

We have measured the temperature-dependent resistivity $\rho(T)$ on a dense pellet [13]. The material is insulating with an activated gap of 0.036 eV. The reduced gap compared to local spin density approximation (LSDA) can arise due to the presence of disorder-induced localized states in the sample.

Using a density response code [22] recently developed for the Elk branch of the original EXCITING FP-LAPW code [23], we derive low-energy effective models represented with the Wannier functions, the interaction parameters for which are evaluated by the contrained RPA [13]. To evaluate the AF coupling through the direct overlap between d orbitals, we first investigate a low-energy effective model for the Ru t_{2g} and O p bands in the energy window $[-7.0{:}+1.0]$ eV. We obtain the onsite Hubbard $U_d = 5.3$ eV and the largest transfer hopping between d orbitals $t_{dd} = 0.19$ eV, which result in a small AF coupling, $J \sim 4t_{dd}^2/U_d = 0.03$ eV.

We also derive an effective model only for the Ru t_{2g} bands in the energy window $[-1.4{:}+1.0]$ eV. In this model, the Wannier functions are the Ru t_{2g} orbitals hybridized with the surrounding O p orbitals, which allows a direct evaluation of the superexchange couplings. We obtain the on-site Hubbard $U = U(\mathbf{r} = 0) = 2.7$ eV, the Hund's coupling $J_H = J(\mathbf{r} = 0) = 0.28$ eV, the nearest-neighbor off-site Coulomb interaction $V = 1.1$ eV, and the largest nearest-neighbor transfer hopping $t = 0.28$ eV. For the AF superexchange coupling, these values result in $J_{AF} \sim 4t^2/(U - V) = 0.20$ eV. On the other hand, the F superexchange coupling J_F is evaluated as the nearest-neighbor off-site direct exchange $\sim$0.03 eV. The superexchange AF coupling J_{AF} dominates over J and J_F. These estimates are replaced by an exact treatment in the following analysis.

In the atomic limit, each site has an $S = 3/2$ spin. When the two sites are coupled, the eigenstates can be labeled by the total spin $S = 0,1,2,3$. Using the effective values of t, U, and J_H in the t_{2g} effective model [13], we perform exact diagonalization for two sites to obtain the energies of states labeled by S. These eigenvalues determine the exchange constants of a general effective spin-3/2 Hamiltonian for two sites as $H_{\text{eff}} = E_0 + J_1(\vec{S}_1 \cdot \vec{S}_2) + J_2(\vec{S}_1 \cdot \vec{S}_2)^2 + J_3(\vec{S}_1 \cdot \vec{S}_2)^3$. We find $J_1 = 45.6$, $J_2 = -2.0$, and $J_3 = 0.5$ meV. The interaction at the two-site level is then primarily Heisenberg AF.

For purposes of modeling the system, we retain the Heisenberg AF nearest neighbor interactions within the plane ($J_\parallel$, 3 neighbors) taken as J_1. Also, motivated by the experimental observation of G-type ordering, we introduce, in addition, a coupling between nearest neighbor planes ($J_\perp$, 2 neighbors). The classical Hamiltonian describing magnetism in $SrRu_2O_6$ is given by

$$H_{\text{classical}} = J_\parallel \sum_{\langle ij \rangle_\parallel} \vec{S}_i \cdot \vec{S}_j + J_\perp \sum_{\langle ij \rangle_\perp} \vec{S}_i \cdot \vec{S}_j. \qquad (1)$$

For $J_\perp = 0$, according to the Mermin-Wagner theorem, the long-wavelength spin waves destroy the long-range order and, consequently, the transition temperature tends to zero in the thermodynamic limit. However, a small interplane coupling can stabilize magnetic order. Our DFT calculations show that the interplane hopping parameters are small with respect to the in-plane parameters ($t_\perp/t_\parallel \sim 0.1$), which suggests that the AF interplane couplings $J_\perp$ are between $0.1J_\parallel$ and $0.01J_\parallel$.

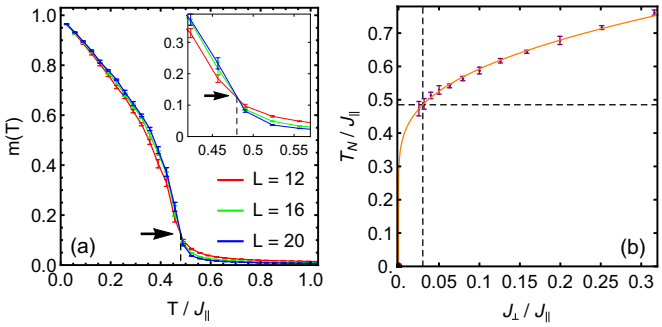

FIG. 4. (Color online) (a) Classical Monte Carlo simulations using the model in Eq. (1) show the staggered magnetization per site vs temperature for $J_\perp/J_\parallel = 0.03$ using three system sizes of linear length L. The transition temperature $T_N = 0.48J_\parallel$ is obtained by locating the intersection of the curves with different system sizes. An enhanced plot near this point is given in the inset. Arrows point to the intersection point, and the corresponding transition temperature is indicated with dotted lines. (b) Transition temperature T_N in units of $J_\parallel$ is plotted as a function of the ratio between the interplane and in-plane couplings. The horizontal dotted line shows the value of $T_N/J_\parallel = 0.48$ from comparing $T_N = 565$ K from experiment with $J_\parallel = 1190$ K from theory. A vertical dotted line shows the corresponding value of $J_\perp/J_\parallel = 0.03$. A fit to $J_\parallel/T_N = \alpha_1 + \alpha_2 \log J_\parallel/J_\perp$ from Ref. [24] using fitting parameters $\alpha_1 = 0.97$ and $\alpha_2 = 0.31$ is given as a solid line.

We perform classical Monte Carlo simulations on a layered honeycomb lattice to obtain the transition temperature as a function of the ratio of these coupling constants. Figure 4 gives the results of these simulations.

The transition temperature obtained from Monte Carlo $T_N^{\mathrm{MC}}(J_\parallel, J_\perp)$ depends on the in-plane and interplane couplings in general as seen in Fig. 4. Using our estimated value for J_1 obtained from downfolding and exact diagonalization, we obtain the AF Heisenberg spin-3/2 coupling constant $J_\parallel = (3/2)^2 J_1 = 102.6$ meV or 1190 K. Further, by using the experimental transition temperature of 565 K, we find that $J_\perp = 36$ K or equivalently $J_\perp/J_\parallel \approx 0.03$ fits the experimental results. The theoretical results also suggest that the transition temperature can be enhanced by increasing the in-plane coupling, for example, by chemical or applied pressure.

As illustrated in the inset of Fig. 1, the quasi-two-dimensional crystal structure of $SrRu_2O_6$ distinguishes itself from other reported high-T_c compounds with a perovskite structure. With the nonmagnetic Sr spacing layers, the interplane coupling is expected to be weak. This is supported by our Monte Carlo simulations. The interplane coupling is small, but critical for the three-dimensional magnetic order. The strong in-plane magnetic interaction is dominated by the AF superexchange coupling between rutheniums, mediated by oxygen. We notice in Fig. 1 only one weak slope change around T_N and also the magnetic susceptibility increases linearly with increasing temperature above T_N. The absence of a Cure-Weiss-like paramagnetic behavior above T_N suggests that strong two-dimensional magnetic fluctuations exist above T_N and persist until this compound decomposes around 800 K.

Our theoretical modeling highlights the mechanism for the high AF temperature. Similar to the mechanism for the perovskite $SrTcO_3$ in Ref. [2], we find that $SrRu_2O_6$ is close to the fluctuating regime with $U \sim W$ on the localized side. This is facilitated by substantial hybridization between Ru $4d$ and O $2p$ within the unit cell as seen from the projected density of states in Fig. 3(b) that reduces the effective U. In addition the hybridization between unit cells enhances the band width W, bringing this material close to the crossover region where T_N is enhanced. Thus, the large covalency reduces the Ru moment but also facilitates a strong (in-plane) AF superexchange interaction, which is important for the high T_N.

With multiple t_{2g} orbitals and Coulomb correlations that generate antiferromagnetism with high ordering temperatures on a honeycomb lattice, it is possible that this material has interesting topological properties that still need to be explored, especially as we replace Ru with the heavier Os and spin-orbit coupling becomes important. It could also be a parent material to explore the possibility of superconductivity upon doping at Sr and Ru sites or changing the oxygen nonstoichiometry. $SrRu_2O_6$, therefore, provides a new materials platform for studying the mechanism inducing high-temperature magnetic order and other exotic phenomena in $4d$ and $5d$ transition-metal oxides.

Note added. Recently, we became aware of the paper by Hiley *et al.* [25], which has substantial similarities with ours but also important differences on two theoretical points. First, unlike Ref. [25], we find that T_N vanishes in the $J_\perp/J_\parallel = 0$ limit, as required by the Mermin-Wagner theorem in two dimensions. Second, our theoretical prediction for the gap is an order of magnitude smaller than Ref. [25], and is in agreement with the recent estimates of Streltsov *et al.* [26] and Singh [27].

Work at ORNL was supported by the U.S. Department of Energy, Office of Science, Basic Energy Sciences, Materials Sciences and Engineering Division (synthesis and characterization) and Scientific User Facilities Division (neutron diffraction). The theoretical modeling (C.S. and N.T.) was supported by the CEM and NSF MRSEC under Grant No. DMR-1420451. R.A. thanks S. Sakai and Y. Nomura for a fruitful discussion. J.G.C. is supported by the National Basic Research Program of China (Grant No. 2014CB921500), the National Science Foundation of China (Grant No. 11304371), and the Strategic Priority Research Program (B) of the Chinese Academy of Sciences (Grant No. XDB07020100).

[1] E. E. Rodriguez, F. Poineau, A. Llobet, B. J. Kennedy, M. Avdeev, G. J. Thorogood, M. L. Carter, R. Seshadri, D. J. Singh, and A. K. Cheetham, Phys. Rev. Lett. **106**, 067201 (2011).

[2] J. Mravlje, M. Aichhorn, and A. Georges, Phys. Rev. Lett. **108**, 197202 (2012).

[3] V. S. Borisov, I. V. Maznichenko, D. Böttcher, S. Ostanin, A. Ernst, J. Henk, and I. Mertig, Phys. Rev. B **85**, 134410 (2012).

[4] C. Franchini, T. Archer, J. He, X.-Q. Chen, A. Filippetti, and S. Sanvito, Phys. Rev. B **83**, 220402(R) (2011).

[5] S. Middey, A. K. Nandy, S. K. Pandey, P. Mahadevan, and D. D. Sarma, Phys. Rev. B **86**, 104406 (2012).

[6] G. Thorogood, M. Avdeev, M. L. Carter, B. J. Kennedy, J. Ting, and K. S. Wallwork, Dalton Trans. **40**, 7228 (2011).

[7] O. N. Meetei, O. Erten, M. Randeria, N. Trivedi, and P. Woodward, Phys. Rev. Lett. **110**, 087203 (2013).

[8] H. Kato, T. Okuda, Y. Okimoto, Y. Tomioka, Y. Takenoya, A. Ohkubo, M. Kawasaki, and Y. Tokura, Appl. Phys. Lett. **81**, 328 (2002).

[9] Y. Krockenberger, K. Mogare, M. Reehuis, M. Tovar, M. Jansen, G. Vaitheeswaran, V. Kanchana, F. Bultmark, A. Delin, F. Wilhelm, A. Rogalev, A. Winkler, and L. Alff, Phys. Rev. B **75**, 020404(R) (2007).

[10] Y. G. Shi, Y. F. Guo, S. Yu, M. Arai, A. A. Belik, A. Sato, K. Yamaura, E. Takayama-Muromachi, H. F. Tian, H. X. Yang, J. Q. Li, T. Varga, J. F. Mitchell, and S. Okamoto, Phys. Rev. B **80**, 161104(R) (2009).

[11] S. Calder, V. O. Garlea, D. F. McMorrow, M. D. Lumsden, M. B. Stone, J. C. Lang, J.-W. Kim, J. A. Schlueter, Y. G. Shi, K. Yamaura, Y. S. Sun, Y. Tsujimoto, and A. D. Christianson, Phys. Rev. Lett. **108**, 257209 (2012).

[12] C. I. Hiley, M. R. Lees, J. M. Fisher, D. Thompsett, S. Agrestini, R. I. Smith, and R. I. Walton, Angew. Chem., Int. Ed. Engl. **53**, 4423 (2014).

[13] See Supplemental Material at http://link.aps.org/supplemental/10.1103/PhysRevB.92.100404 for (1) experimental details, (2) refinement of the neutron diffraction pattern taken at 300 K, (3) temperature dependence of electrical resistivity, and (4) band structure and DOS for AF state.

[14] R. M. Moon, T. Kiste, and W. C. Koehler, Phys. Rev. **181**, 920 (1969).

[15] Q. Huang, P. Karen, V. L. Karen, A. Kjekshus, J. W. Lynn, A. D. Mighell, N. Rosov, and A. Santoro, Phys. Rev. B **45**, 9611 (1992).

[16] J. W. Lynn, N. Rosov, and G. Fish, J. Appl. Phys. **73**, 5369 (1993).

[17] J. B. Goodenough, Phys. Rev. **100**, 564 (1955); J. Phys. Chem. Solids **6**, 287 (1958).

[18] J. Kanamori, J. Phys. Chem. Solids **10**, 87 (1959).

[19] P. Blaha *et al.*, http://www.wien2k.at.

[20] J. P. Perdew and Y. Wang, Phys. Rev. B **45**, 13244 (1992).

[21] We call the Ru-*d* bands near the Fermi energy the t_{2g} bands for convenience, whereas the t_{2g} bands experience an additional crystal field splitting in this material. However, it is just a unitary transformation of the basis in our model and so does not affect the following analysis.

[22] A. Kozhevnikov, A. G. Eguiluz, and T. C. Schulthess, in *SC10 Proceedings of the 2010 ACM/IEEE International Conference for High Performance Computing, Networking, Storage, and Analysis, New Orleans, LA, USA - Nov. 13-19, 2010* (IEEE Computer Society, Washington, DC, USA, 2010), pp. 1–10.

[23] J. Spitaler *et al.*, The EXCITING FP-LAPW code, http://exciting.sourceforge.net/.

[24] K. Lee, J. Magn. **6**, 119 (2001).

[25] C. I. Hiley, D. O. Scanlon, A. A. Sokol, S. M. Woodley, A. M. Ganose, S. Sangiao, J. M. De Teresa, P. Manuel, D. D. Khalyavin, M. Walker, M. R. Lees, and R. I. Walton, Phys. Rev. B **92**, 104413 (2015).

[26] S. Streltsov, I. I. Mazin, and K. Foyevtsova, arXiv:1508.02370.

[27] D. J. Singh, Phys. Rev. B **91**, 214420 (2015).